·Article·
Advances in Polar Science
doi: 10.3724/SP.J.1085.2013.00012
March 2013 Vol. 24 No. 1: 12-18

Study of ionospheric disturbances during solar flare events using the SuperDARN Hokkaido radar

Daiki Watanabe* & Nozomu Nishitani

Solar-Terrestrial Environment Laboratory, Nagoya University, Nagoya 464-8601, Japan

Received 31 August 2012; accepted 7 January 2013

Abstract It is well known that many types of ionospheric disturbances occur during solar flare events. The sudden increase in total electron content (SITEC) has been studied for several decades, but total electron content (TEC) data do not provide information on the altitudinal distribution of electron density changes. Previous studies used HF Doppler system data to investigate the contributions of the D-region and F-region ionospheric electron density changes by examining the HF radio wave frequency dependence on the Doppler shift values. In this study we examined the dependence of the elevation angle of the Doppler shift of ground scatter echoes using the SuperDARN Hokkaido radar. We analyzed solar flare events from Dec 2006 to Mar 2012. A sudden fade-out of echoes was observed in almost all the events we analyzed, which was the result of the radio absorption associated with a significant increase in electron density within the D-region ionosphere. In addition, we discovered positive Doppler shifts just before the sudden fade-out of echoes. The Doppler shift is negatively correlated with the elevation angle of received radar waves. It indicates that variation of electron density in the D-region ionosphere is dominant during solar flare events. This result is consistent with a previous study. We also compared the irradiation by X-ray and extreme ultra violet rays observed by the GOES-14 and GOES-15 satellites, which generated Doppler shifts. A positive Doppler shift is consistent with a change of X-ray flux.

Keywords **solar flare, SuperDARN Hokkaido radar, Doppler shift, D-region, F-region, GOES satellite**

Citation: Watanabe D, Nishitani N. Study of ionospheric disturbances during solar flare events using the SuperDARN Hokkaido radar. Adv Polar Sci, 2013, 24:12-18, doi: 10.3724/SP.J.1085.2013.00012

1 Introduction

During solar flare events, X-ray, extreme ultra violet (EUV) rays and high energy particles bombard the Earth. As a result, ionospheric disturbances occur, such as a total electron content increase and radio wave absorption. Solar flares are classified in terms of intensity of soft X-ray (1.0–8.0 Å) radiation. During solar flare events, X-ray flux increases in intensity by up to 1 000 times, and EUV flux increases by several tens of percentage. EUV radiation ionizes the whole ionosphere and soft X-ray radiation ionizes the region under the E-region ionosphere[1].

Kikuchi et al.[2] described using the HF Doppler system data in which Doppler shifts in HF radio waves during solar flare events are caused by two factors, and discussed the importance of both factors. One is the apparent decrease in the ray path as a result of the change in the refraction index caused by increasing electron densities in the D-region (non-deviating slab) ionosphere (factor A). The other is the ray path decrease because of the descending reflection point associated with increasing electron density in the F-region ionosphere (factor B). Figure 1 illustrates the cases for factors A and B with the change in X-ray and EUV flux.

These factors were originally described quantitatively by Davies et al.[3]. Setting the refractive index as n, wave frequency as f, and wavelength as λ, we have:

$$l = \frac{c}{nf}, \tag{1}$$

where c denotes the speed of light. The frequency deviation of the received signal Δf is given by a time derivative of the number of waves on the path s, i.e., s/λ, as:

* Corresponding author (email: dwatana@stelab.nagoya-u.ac.jp)

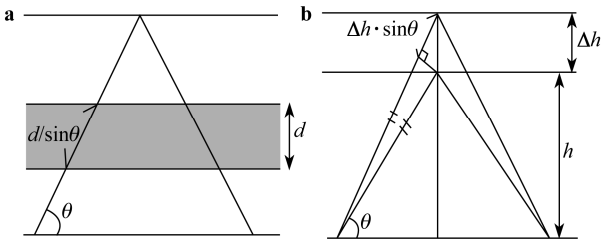

Figure 1 Model of Doppler frequency deviations caused by D-region (nondeviating slab) electron density increase and leading apparent ray path decrease (**a**, factor A) and F-region electron density increase causing reflection height decrease (**b**, factor B).

$$\Delta f = -\frac{\mathrm{d}}{\mathrm{d}t}\left(\frac{s}{l}\right). \tag{2}$$

We define the apparent path P as:

$$P = ns. \tag{3}$$

From Eqs. (1), (2) and (3), we obtain:

$$\Delta f = -\frac{f}{c}\frac{\mathrm{d}P}{\mathrm{d}t}. \tag{4}$$

First, we consider factor A. In this case, the change in refractive index, Δn, is caused by the extra ionization in the D-region ionosphere (non-deviating slab). According to Eq.(3), ΔP is given by:

$$\Delta P = 2\Delta n \cdot \mathrm{d}\frac{1}{\sin q}. \tag{5}$$

From Eqs. (4) and (5), we obtain:

$$\Delta f = -2\frac{f \cdot d}{c} \cdot \frac{\mathrm{d}n}{\mathrm{d}t} \cdot \frac{1}{\sin q}, \tag{6}$$

where d is the thickness of the D-region ionosphere and θ is the elevation angle.

If we ignore the presence of the geomagnetic field and collisions between electrons and neutral particles, the refractive index n is expressed by:

$$n^2 = 1 - \frac{kN}{f^2}, \tag{7}$$

where k=8.06×10^{-11} m^3·s^{-2}. Accordingly, Δn is described as:

$$\Delta n = -\frac{1}{2} \cdot k \cdot \frac{\Delta N}{f^2}. \tag{8}$$

By substituting Eq. (8) into Eq. (6), we obtain:

$$\Delta f = \frac{k \cdot d}{c \cdot f} \cdot \frac{\mathrm{d}N}{\mathrm{d}t} \cdot \frac{1}{\sin q}. \tag{9}$$

From Eq. (9), we note that Δf is inversely proportional to f and sinθ.

In case of factor B, the changing reflecting height is caused by extra ionization in the F-region ionosphere. Presuming that $\Delta h << h$, ΔP is given by:

$$\Delta P = 2 \cdot \Delta h \cdot \sin q, \tag{10}$$

where h is reflecting height. Substituting Eq. (10) into Eq. (4), we obtain:

$$\Delta f = -2\frac{f}{c} \cdot \frac{\mathrm{d}h}{\mathrm{d}t} \cdot \sin q, \tag{11}$$

Note that Δf is proportional to f and to sinθ for case B.

Kikuchi et al.[2], using the HF Doppler technique, analyzed the frequency dependence of the HF wave Doppler shift during solar flare events in 1982. They found that there were cases where the Doppler shift was inversely proportional to f. This result indicated that the significant change in electron density in the D-region ionosphere is dominant during solar flare events. However, there were a few events where the Doppler shift was proportional to f, so they could not reach a firm conclusion.

Doppler shift also depends on the elevation angle θ. Kikuchi et al.[2] could not analyze elevation angle dependence because the transmitter and receiver positions of the HF Doppler system were fixed so that the ray path geometry was very limited. In this study we analyze the range and elevation angle dependence of the HF wave Doppler shift during solar flare events using the SuperDARN Hokkaido radar. We also analyze the variations of the irradiation of X-ray and EUV during solar flare events and compare them with the Doppler shift of the radar echoes.

2 Data analysis

We used the SuperDARN Hokkaido radar[4] data for the analysis. This radar is one of the SuperDARN radars and is located at the lowest geomagnetic latitude for these radars. The radar field of view is shown in Figure 2. The advantage of these geographical characteristics is that it is relatively easy to detect solar flares because of the relatively small solar zenith angle. The temporal resolution is 1 s–2 min, spatial resolution 15–45 km and peak power 10 kW.

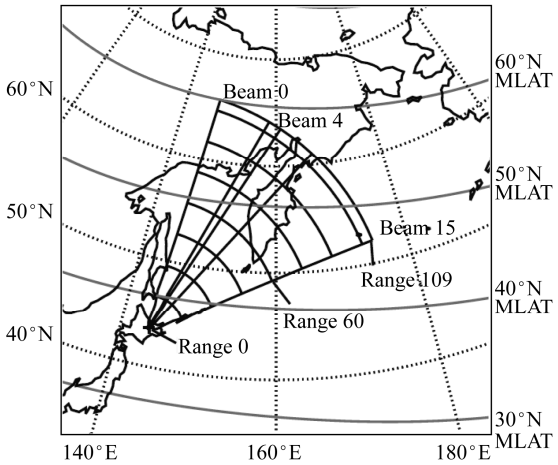

Figure 2 Field of view of the SuperDARN Hokkaido Radar.

Radar echoes are classified into two categories (Figure 3). One is the ionospheric scatter echo where radar waves are backscattered by ionospheric irregularities. The other is ground scatter echoes where radar waves are reflected at the ionosphere (or the Earth's surface) and backscattered by irregular structures of the Earth's surface. Generally ground scatter echoes have small Doppler shifts and small Doppler spectral widths[5]. In this study we focus on ground/sea

scatter echoes with 1 hop geometry[6-7], as shown in Figure 3.

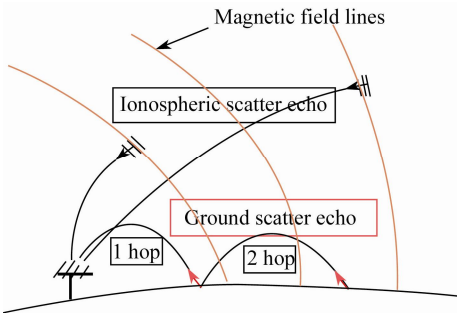

Figure 3 Illustration of two kinds of echo receiption geometry.

We obtain three types of parameters (echo power, Doppler velocity and Doppler spectral width) from the Doppler spectra of radar echoes. In this study, we analyze the Doppler velocity parameter. The Doppler velocity v is given by[8]:

$$v = \frac{c\Delta f}{2 \cdot f}. \quad (12)$$

In case of factor A, from Eqs. (9) and (12), v is given by:

$$v = \frac{k \cdot d}{f^2} \cdot \frac{\mathrm{d}N}{\mathrm{d}t} \cdot \frac{1}{\sin q}. \quad (13)$$

In case of factor B, from Eqs. (11) and (12), we obtain:

$$v = -2\frac{\mathrm{d}h}{\mathrm{d}t}\sin q. \quad (14)$$

Factors A and B affect the Doppler shift separately and simultaneously, so v is described as follows:

$$v = \frac{k \cdot d}{f^2} \cdot \frac{\mathrm{d}N}{\mathrm{d}t} \cdot \frac{1}{\sin q} - 2\frac{\mathrm{d}h}{\mathrm{d}t}\sin q. \quad (15)$$

The radar data also contain elevation angle information, which is derived from the phase difference in the main and interferometer array signals (e.g., Milan et al.[9]). There is usually a hardware offset in the phase difference parameter and consequently the elevation angle data may contain errors. Usually the parameter is calibrated by technical experiments or the observation of meteor echoes. Unfortunately the Hokkaido radar data have not yet been fully calibrated. Therefore we calculate the elevation angle (proxy value) from the slant range information. Figure 4 shows a simple model used for calculating elevation angle (proxy). Assuming the reflecting height is constant at 250 km, θ is calculated as follows:

$$q = \arcsin\frac{250}{l/2}. \quad (16)$$

Strictly speaking, the reflecting height increases slightly with the elevation angle at a fixed frequency. According to the ray path calculation result using the model ionosphere by Nishitani and Ogawa[4], the reflection height is about 250 km at the ground backscatter range of 700 km whereas it is about 200 km at a range of 1 800 km during daytime under disturbed conditions. Under these conditions, there is an approximately 3° elevation angle error at a range of 1 800 km in our model. However, we confirmed that consideration of this height change does not affect our results for the evaluation of factors A and B.

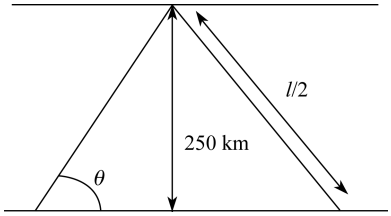

Figure 4 A simple model of calculating the elevation angle proxy value based on the slant range reflection assumed height and radar wave path geometry.

Together with the Hokkaido radar data, we use X-ray and EUV radiation data observed by the GOES-14 and GOES-15 satellites in geosynchronous orbit. The temporal resolution of the data used in this study is 1 min.

The flares from Dec 2006 to Apr 2012 meeting the following criteria are surveyed for this analysis. (1) The flare class is larger than M 2.0. (2) The flare occurred from 0600 to 1800 Japan Standard Time (JST). In the next section we focus on the result of the event analysis, with some description of the statistical survey.

3 Results

3.1 Event study

Here we study two solar flare events where the ionospheric effect of the solar flare was clearly registered.

3.1.1 Event on 9 Mar 2012

First we describe the solar flare event that occurred on 9 Mar 2012. The top panel of Figure 5 presents the temporal variation of the Doppler velocity observed from beam 4. During this event the radar was operating in the "themisscan" mode, where the camping beam 4 was sampled every 8 s. The first range gate and range resolution were 180 km and 45 km. The vertical axis shows the range gate. The color scale is from −30 m·s^{-1} to 30 m·s^{-1} where blue corresponds to positive values (towards the radar) and red to negative values (away from the radar). The horizontal axis gives universal time (UT) (JST=UT+9 h). The second and third panels show the radiation of X-ray and EUV. In the second panel, the black curve is the hard X-ray of 0.5−4.0 Å wavelength (left axis) and the red curve is the soft X-ray, of 1.0−8.0 Å wavelength (right axis). In the third panel, the black curve is EUV of 50−170 Å wavelength (left axis) and the red curve is for 304 Å wavelength. It is clear that positive variation of the Doppler velocity occurred twice, at 0325 UT and 0330 UT. At the same time, the X-ray and EUV irradiations increased. A sudden fade-out of echoes was observed just after the positive Doppler velocity. This fade-out is likely to be caused by

radio wave absorption because of an extra increase in the D and E-region electron densities. To study this Doppler shift in more detail, we analyze its range and elevation angle (proxy) dependence between 0325 UT and 0326 UT.

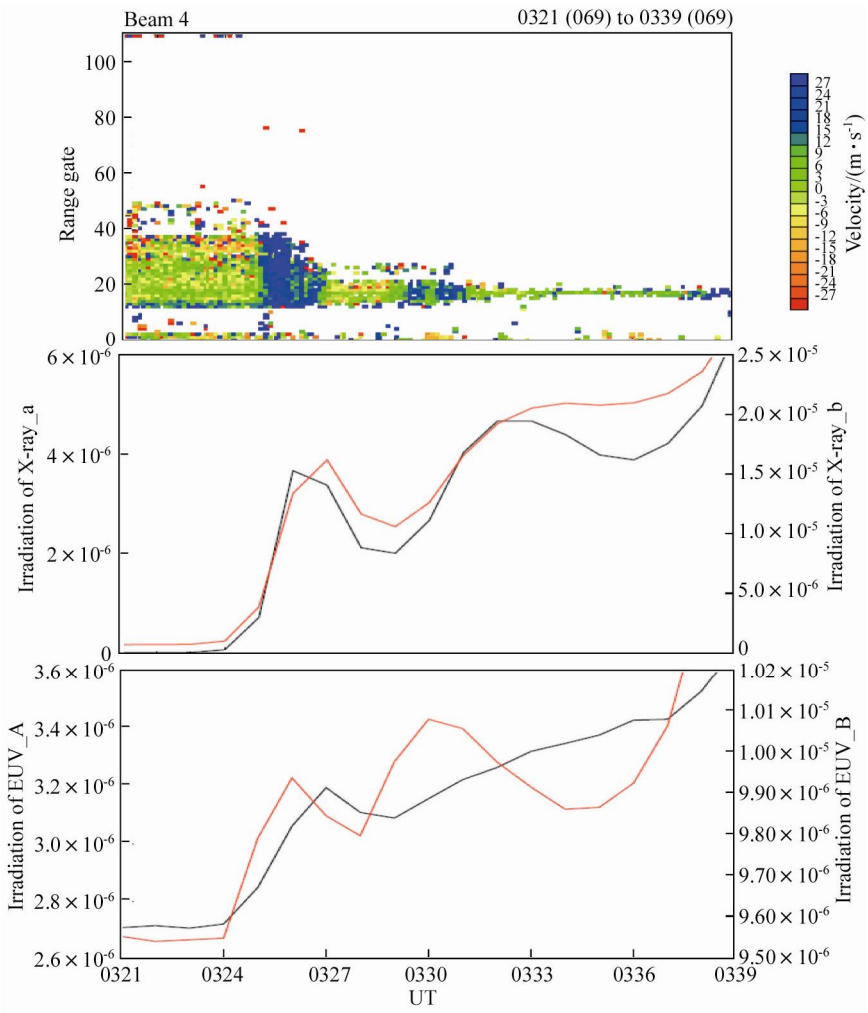

Figure 5 Temporal variation of Doppler velocity observed by the SuperDARN Hokkaido radar, together with X-ray and EUV flux on 9 March 2012.

Figure 6 shows the relationship between the Doppler velocity (vertical axis) and range gate (horizontal axis). The parameters for beam 0 to beam 7 are superimposed to add the data points. We confirmed that the beam number dependence on the Doppler velocity is relatively small. It is apparent that Doppler velocity is faster for longer ranges, especially from range gates 20 to 40.

Figure 7 shows the relationship between Doppler velocity (vertical axis) and elevation angle proxy value (horizontal axis) calculated using the method described in the previous section (Eq. (16)). The red line is the fitting curve, which will be described later in this section. Parameters are confined from range gates 20 to 40 because, judging from the continuity of values, including the observed elevation angle values with hard offset (not shown here), it is certainly in this range that echoes can be regarded as 1-hop ground scatter echoes. We can say that the Doppler velocity is faster for a smaller elevation angle (proxy). These range and elevation angle dependencies may indicate that the effect of increasing electron densities in the D-region ionosphere (non-deviating slab) is dominant.

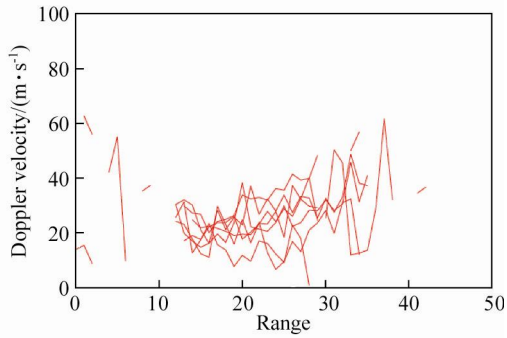

Figure 6 Plot of Doppler velocity versus range gate at 0325 UT, 9 March 2012.

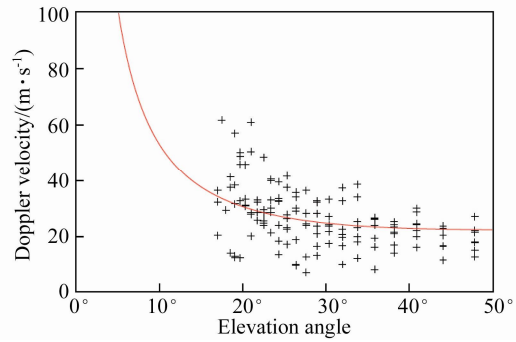

Figure 7 Scattered plot of the Doppler velocity versus elevation angle proxy value at 0325 UT, 9 March 2012. The red curve show the result of fitting to Eq. (17).

As described before, the Doppler velocity is given by Eq. (15), so we can fit the data points of Figure 7 into:

$$v = a \times \frac{1}{\sin q} + b \times \sin q \ , \tag{17}$$

and obtain the red curve:

$$v = 8.80 \times \frac{1}{\sin q} + 14.12 \times \sin q \ . \tag{18}$$

For the elevation angle of 10° to 40° where most of the data exist, $\sin\theta$ is smaller than $1/\sin\theta$, therefore it is presumed that the second term of Eq. (18) is generally negligible. Furthermore, considering the propagation of errors in v, we found that errors in a are relatively small and in b relatively large. Therefore it is difficult to assess value b quantitatively. Thus, we discuss only value a. There are also errors because of the difference in reflection height for different ranges. However, we confirmed that the effect of this error is negligible in evaluating value a.

Comparing Eq. (16) with Eq. (9):

$$\frac{k \cdot d}{f^2} \cdot \frac{\mathrm{d}N}{\mathrm{d}t} = 8.80 \ . \tag{19}$$

Thus we can estimate the variation in the D-region electron density with a few assumptions. Assuming that k=8.06×10^{-11} $m^3 \cdot s^{-2}$, f=11 MHz, d=30×10^3 m, we obtain dN/dt= 4.40×10^8 $m^{-3} \cdot s^{-1}$ (detailed discussion in the next section).

We show the temporal variation in echo power in Figure 8. The top panel is the Doppler velocity and the second panel is the echo power for several range gates. The echo power started decreasing when positive Doppler velocity occurred. This is consistent with results showing that the D-region electron density change is dominant.

3.1.2 Event on 9 Aug 2011

We next analyze the solar flare event that occurred on 9 Aug 2011. During this period the radar was operating in the "normalscan" mode, sequentially sampling beams 15, 14, ..., 1 and 0 with a 3 s integration time for each beam, and sampling the whole field of view every 1 min. The first range gate and range resolution were 180 km and 45 km. The top panel of Figure 9 shows the temporal variation of the Doppler velocity observed by all beam directions, and the second and third panels show the temporal changes in radiation for X-ray and EUV. The positive Doppler velocity began when the solar irradiation started increasing (0802 UT).

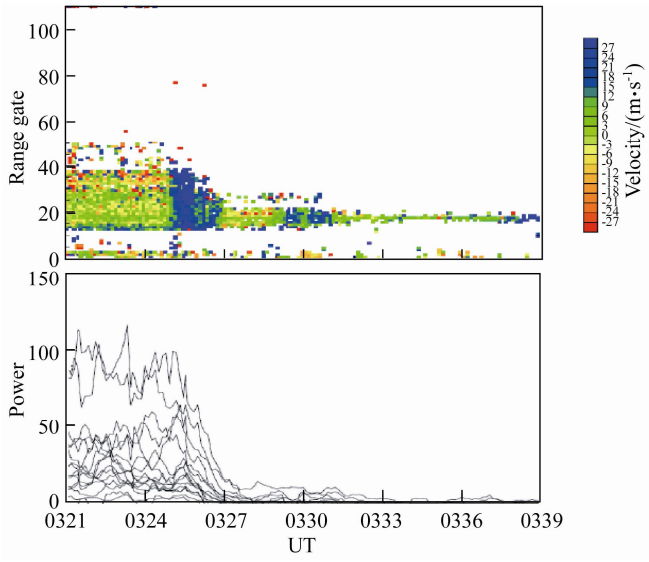

Figure 8 Temporal variation of echo power (lower panel) compared with the Doppler velocity (upper panel) on 9 March 2012.

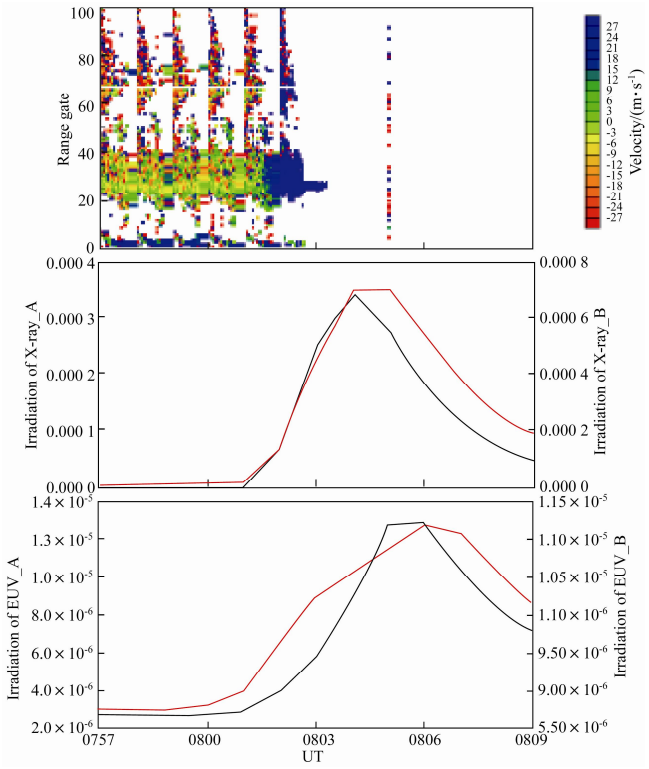

Figure 9 Temporal variation of Doppler velocity observed by the SuperDARN Hokkaido radar, together with X-ray and EUV flux on 9 August 2011.

Figure 10 shows the relationship between the Doppler velocity and range gate, and Figure 11 shows the relation-

ship between the Doppler velocity and elevation angle proxy when positive Doppler velocity occurred (0802 UT to 0803 UT). The Doppler shift has a positive correlation to the range and a negative correlation to the elevation angle proxy.

We obtain the fitting curve (red curve in Figure 11):

$$v = 24.9 \times \frac{1}{\sin q} + 18.4 \times \sin q \ , \qquad (20)$$

which yields $dN/dt=1.24\times10^{9}$ $m^{-3}\cdot s^{-1}$ in the same way as in the previous event. We considered only the value a for the same reason as in the previous event.

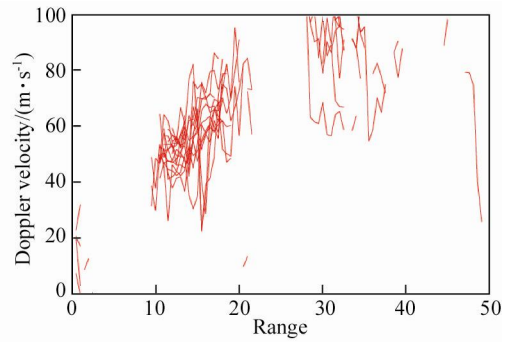

Figure 10 Plot of Doppler velocity versus range gate at 0802 UT, 9 August 2011.

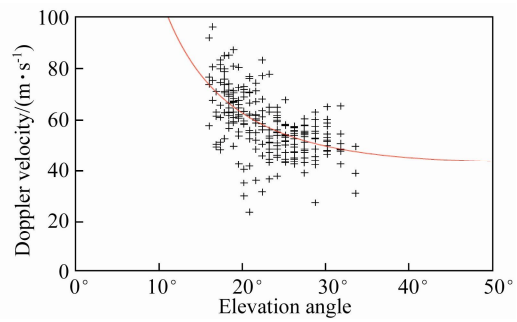

Figure 11 Scattered plot of the Doppler velocity versus elevation angle proxy value at 0802 UT, 9 August 2011. The red curve show the result of fitting to Eq. (17).

3.2 Statistical study

We performed statistical analyses of flare events larger than M 2.0 from Dec 2006 to Mar 2012, for 0600–1800 LT (total number: 29). Among them, 24 events showed clear positive Doppler shifts for the ground scatter echoes. Of these 24 events, 11 showed a positive range dependence on the Doppler shift. This result indicates that the D-region electron density change is a dominant factor during solar flare events. The other 13 events did not show obvious range dependence. This might suggest that there is some effect from the F-region electron density changes but it is significantly smaller than the D-region effect, or the effect of noise scattering Doppler velocities.

4 Discussion and conclusions

We analyzed solar flare events using the SuperDARN Hokkaido radar. We succeeded in establishing range and elevation angle dependence on the HF wave Doppler shift, which could not be analyzed using the previous HF Doppler method. We also used X-ray and EUV flux data. Obviously there was a correlation between the radiation flux and Doppler shift changes.

In Figure 5, positive Doppler velocity was registered at the time X-ray and EUV flux was increasing. When the flux was decreasing or unchanged, positive Doppler velocity was not registered. Therefore, this change in Doppler velocity corresponds to an increased rate of solar irradiation. In Figure 9, positive Doppler velocity was also registered when the X-ray and EUV flux was increasing. This change in Doppler velocity was likely to be caused by the two factors A and B as previously described. In both events, the Doppler velocity shows positive correlation with the range in Figures 6 and 10, and negative correlation to the elevation angle in Figures 7 and 11. This dependence is characteristic of factor A. Thus, we can say that this Doppler shift was caused mainly by the increasing D-region (non-deviating slab) electron density. This is consistent with the results of Kikuchi et al.[2].

Figure 8 indicates that the positive Doppler shift and echo power decrease began simultaneously. Decreasing echo power is most likely caused by radio absorption with the extra increase in D-region electron density. Therefore, this might be additional supporting evidence that increasing electron density in the D-region is a more dominant factor than in the F-region.

In the other 13 events, Doppler shift also has positive range dependence and negative elevation angle dependence. Although the other 13 events show scattered relationships, no event shows that the Doppler shift has a negative correlation to the range or positive correlation to the elevation angle. Therefore, there was no possibility in the events we analyzed that the electron density variation in the F-region ionosphere was more dominant than in the D-region.

We estimated the amount of electron density change in the D-region from the fitting curves. The value obtained for the event on 9 Mar 2012 was $dN/dt=4.40\times10^{8}$ $m^{-3}\cdot s^{-1}$ and that obtained for the event on 9 Aug 2011 was $dN/dt=1.24\times10^{9}$ $m^{-3}\cdot s^{-1}$. Kikuchi et al.[2] estimated $d(Nd)/dt=2\times10^{13}$ $m^{-3}\cdot s^{-1}$, i.e., $dN/dt=6.67\times10^{8}$ $m^{-3}\cdot s^{-1}$, for their event on 5 June 1982. Both events we analyzed showed values consistent with Kikuchi et al.[2]. The value obtained for the event on 9 Aug 2011 was larger than for the event on 9 Mar 2012. We do not discuss the electron density change of the F-region ionosphere because of large errors in the value b. We need more precise observation for detailed discussion on this factor.

We also compared the estimated electron density changes with the variation in X-ray and EUV irradiation. For the event on 9 Mar 2012, X-ray and EUV irradiation change rates (at 0325 UT) were $dI/dt=9.53\times10^{-6}$ $W\cdot m^{-2}$ and $dI/dt=2.13\times10^{-7}$ $W\cdot m^{-2}$. For the event on 9 Aug 2011, X-ray and EUV radiation change rates (0802 UT) were $dI/dt=3.05\times10^{-4}$ $W\cdot m^{-2}$ and $dI/dt=1.84\times10^{-6}$ $W\cdot m^{-2}$. The values

were larger for the event on 9 Aug 2011. This difference was consistent with the Doppler shift difference.

Examining Figures 5 and 9 carefully, we find that positive change in the Doppler shift is likely to correspond more closely to increasing X-ray flux than increasing EUV flux. X-ray and EUV ionize different regions of the ionosphere, so the Doppler shift was probably generated in the region where the X-ray ionized. This suggestion is consistent with the result that the D-region electron density increase is dominant. To reach a firm conclusion, we need to study more events statistically.

In conclusion, during solar flare events, the electron density increase in the D-region ionosphere is dominant and the amount of electron density change corresponds to the solar flux change. Of course these characteristics may depend on local time, season and solar zenith angle. We need to analyze these characteristic more statistically. This is a subject for future study.

Acknowledgements We would like to thank all the staff who contributed to the HF radar experiment at Hokkaido. The X-ray radiation data were provided by National Geophysical Data Center (NGDC) of NOAA and the EUV radiation data were provided by the Laboratory for Atmospheric and Space Physics (LASP) of Colorado University. This work was supported by a Grant-in-Aid for Scientific Research, of the Ministry of Education, Culture, Sports, Science and Technology of Japan (Grant no. 19340141), and also by Special Funds for Education and Research (Energy Transport Processes in Geospace) of the Ministry of Education, Culture, Sports, Science and Technology of Japan.

References

1 Donnelly R F. Empirical model of solar flare X-ray and EUV emission for use in studying their E and F region effects. J Geophys Res, 1976, 81(25): 4745-4753.

2 Kikuchi T, Sugiuchi H, Ishimine T, et al. Solar-terrestrial disturbances of June-September 1982. IV. Ionospheric disturbances. 11. HF Doppler observations. J Radio Res Lab, 1986, 33(1): 239-255.

3 Davies K, Watts J M, Zacharisen D H. A study of F2-layer Effects as Observed with a Doppler Technique. J Geophys Res, 1962, 67(2): 601-609.

4 Nishitani N, Ogawa T. Model calculations of possible ionospheric backscatter echo area for a mid-latitude HF radar. Adv Polar Upper Atmos Res, 2005, 19: 55-62.

5 Ogawa T, Nishitani N, Otsuka Y, et al. Medium Scale Traveling Ionospheric Disturbances Observed with the SuperDARN Hokkaido radar, All-sky imager, and GPS Network and Their Relation to Concurrent Sporadic E Irregularities. J Geophys Res, 2009, 114: 3316-333.

6 Hayashi H, Nishitani N, Ogawa T, et al. Large-Scale traveling ionospheric disturbance observed by the SuperDARN Hokkaido HF radar and GPS networks on 15 December 2006. J Geophys Res, 2010, 115, A06309, doi: 10.1029/2009JA014297.

7 Nishitani N, Ogawa T, Otsuka Y, et al. Propagation of large amplitude ionospheric disturbances with velocity dispersion observed by the SuperDARN Hokkaido radar after the 2011 off the Pacific coast of Tohoku Earthquake. Earth Planets Space, 2011, 63 (7): 891-896, doi:10.5047/eps. 2011.07.003.

8 Baker K B, Dudeney J R, Greenwald, et al. HF radar signatures of the cusp and low-latitude boundary layer. J Geophys Res, 1995, 100(A5): 7671-7695.

9 Milan S E, Jones T B, Robinson T R, et al. Interferometric evidence for the observation of ground backscatter originating behind the CUTLASS coherent HF radars. Ann Geophys, 1997, 15: 29-39.